Australian Journal of Earth Sciences (1999) **46**, 377–389

Geochemistry and geochronology of the Rathjen Gneiss: implications for the early tectonic evolution of the Delamerian Orogen

J. FODEN[1], M. SANDIFORD[1], J. DOUGHERTY-PAGE[1] AND I. WILLIAMS[2]

[1]*Department of Geology, University of Adelaide, SA 5005, Australia.*
[2]*Research School of Earth Sciences, Australian National University, ACT 0200, Australia.*

The Rathjen Gneiss is the oldest and structurally most complex of the granitic intrusives in the southern Adelaide Fold-Thrust Belt and therefore provides an important constraint on the timing of the Delamerian Orogen. Zircons in the Rathjen Gneiss show a complex growth history, reflecting inheritance, magmatic crystallisation and metamorphism. Both single zircon evaporation (`Kober' technique) and SHRIMP analysis yield best estimates of igneous crystallisation of 514 ± 5 Ma, substantially older than other known felsic intrusive ages in the southern Adelaide Fold-Thrust Belt. This age places an older limit on the start of the Delamerian metamorphism and is compatible with known stratigraphic constraints suggesting the Early Cambrian Kanmantoo Group was deposited, buried and heated in less than 20 million years. High-U overgrowths on zircons were formed during subsequent metamorphism and yield a $^{206}Pb/^{238}U$ age of 503 ± 7 Ma. The Delamerian Orogeny lasted no more than 35 million years. The emplacement of the Rathjen Gneiss as a pre- or early syntectonic granite is emphasised by its geochemical characteristics, which show affiliations with within-plate or anorogenic granites. In contrast, younger syntectonic granites in the southern Adelaide Fold-Thrust Belt have geochemical characteristics more typical of granites in convergent orogens. The Early Ordovician post-tectonic granites then mark a return to anorogenic compositions. The sensitivity of granite chemistry to changes in tectonic processes is remarkable and clearly reflects changes in the contribution of crust and mantle sources.

Key words: Adelaide Fold-Thrust Belt, Delamerian Orogeny, granite, radiometric dating, Rathjen Gneiss.

INTRODUCTION

The southern Adelaide Fold-Thrust Belt is part of the Delamerian Orogen formed by convergence along the eastern and southeastern margin of the Gawler Craton during Late Cambrian and Early Ordovician times (Offler & Fleming 1968; Daily & Milnes 1973; Preiss 1987; Coney *et al.* 1990; Jenkins 1990; Jenkins & Sandiford 1992; Flöttmann *et al.* 1994). Most stages of the development of the southern Adelaide Fold-Thrust Belt were accompanied by igneous activity (Figure 1) and the associated magmatic rocks provide a useful chronological framework for the development of the orogen as well as important insights into the role of deeper crustal and mantle processes (J. Foden unpubl. data). In the southern Adelaide Fold-Thrust Belt deformation was immediately preceded by the deposition of the carbonate-rich Normanville Group and the clastic turbidites of the Kanmantoo Group. This Early Cambrian sedimentation was accompanied by small volumes of mafic volcanism which has been interpreted by some workers to reflect an extensional (Preiss 1987) or transpressional (Flöttmann *et al.*1995) tectonic regime. The character of the magmas changed from mafic to felsic (dominantly granitic) by the time of development of the first identifiable tectonic fabrics (Sandiford *et al.* 1992) in the core of the orogen. The immediate post-convergent phase of the orogen was associated with high-level, bimodal igneous activity (Foden *et al.* 1990; Turner & Foden 1990; Turner *et al.* 1992).

The Rathjen Gneiss (Milnes *et al.* 1975; Fleming & White 1984) forms one of a number of variably deformed granitic intrusions in the core of the southern Adelaide Fold-Thrust Belt, some 60 km east of Adelaide (Figures 1, 2). Because of the important role 'granitic' rocks play in the orogenic processes, these felsic orthogneisses and associated granites have received considerable attention in recent discussions of the evolution of the southern Adelaide Fold-Thrust Belt (Milnes *et al.* 1975; Fleming & White 1984; Foden *et al.* 1990; Sandiford *et al.* 1992, 1995; Oliver & Zakowski 1995). All workers agree that the Rathjen Gneiss is particularly important as structural criteria (see below) clearly indicate that it represents the oldest of the felsic igneous suites in this part of the belt. Because of its importance in defining the structural evolution of the belt its absolute age is critical, but has hitherto not been determined. Moreover, opinions also have differed on the nature of its contact relations with surrounding Kanmantoo metasediments (Fleming & White 1984; Sandiford *et al.* 1992) and on the regional significance of the deformational fabrics within the gneiss (Oliver & Zakowski 1995; Sandiford *et al.* 1995). The purpose of this paper is to summarise results of field observations that clarify some of this uncertainty and to present new isotopic and geochemical data pertaining to the age and origin of the Rathjen Gneiss. These new data provide an important framework for discussing the evolution of the early stages of the development of the southern Adelaide Fold-Thrust Belt.

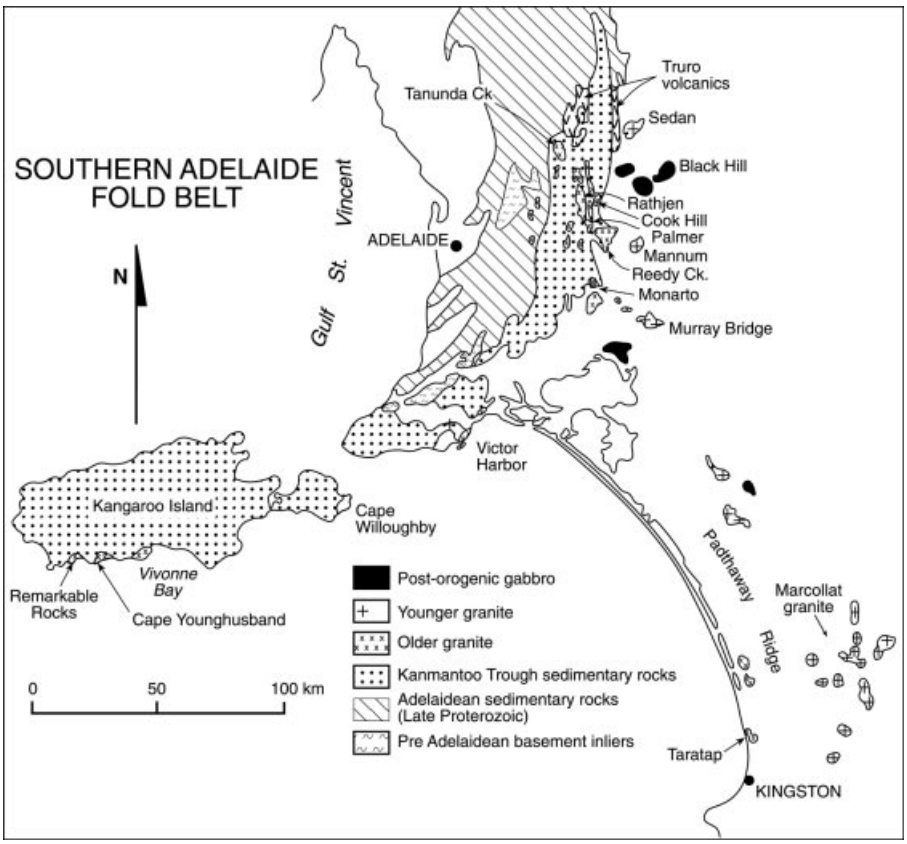

Figure 1 Distribution of igneous rocks in the southern Adelaide Fold-Thrust Belt (after Foden *et al.* 1990).

REGIONAL SETTING AND GEOCHEMISTRY OF THE GRANITES

Granitic rocks in the southern Adelaide Fold-Thrust Belt fall into two broad groups defined on both field and geochemical grounds. An older, syntectonic suite is characterised by tectonic foliations, and clearly pre-dates an undeformed post-tectonic suite intruded after the cessation of Delamerian folding. The syntectonic granites are largely confined to the central, highest metamorphic grade, core of the orogen (Figure 1) in the eastern parts of the Mt Lofty Ranges, the Fleurieu Peninsula and along the south coast of Kangaroo Island. On the basis of field relationships the Rathjen Gneiss is the oldest known Cambrian granite in the belt (see discussion below). Other members of this syntectonic suite include the Palmer, Victor Harbor and Tanunda Creek granites, the Reedy Creek granodiorite and a number of unnamed granites exposed along the south coast of Kangaroo Island near Vivonne Bay.

The post-tectonic granites and associated igneous rocks are largely confined to isolated outliers in the Murray Basin immediately east of the Mt Lofty Ranges between Sedan and Murray Bridge and along the Padthaway Ridge. These include the Murray Bridge, Mannum, Sedan, Padthaway, Christmas Rocks and Mt Monster granites (Turner & Foden 1996). These granites form part of a bimodal suite that includes mafic intrusions at Reedy Creek and in the Black Hill, Sedan, Cambrai area (Turner 1996). The age of the post-tectonic suite is constrained by a number of studies (Milnes *et al.* 1975; Turner 1996; Turner *et al.* 1996) to the range 490–480 Ma and provides a minimum age for the cessation of pervasive Delamerian deformation.

The geochemical distinction between the two suites in the southern Adelaide Fold-Thrust Belt (Table 1) has been highlighted by several authors (Foden *et al.* 1990; Mancktelow 1990; Sandiford *et al.* 1992). The time-dependant transitions of magma types in the Delamerian orogen represent changing proportions of crust and mantle source materials coupled with systematic variation in the extent of fractionation (J. D. Foden unpubl. data). The post-tectonic suite consists of highly fractionated, siliceous A-type granites with low CaO, MgO and Sr abundances, high K_2O and Rb abundances and high K_2O/Na_2O ratios (Figure 4). They have very low Mg and are rich in F, rare-earth elements, Y and Zr (Figures 4, 5). They have characteristics (Turner *et al.* 1992) which imply high-temperature fractionation at low aH_2O, with very late onset of zircon and accessory phase fractionation. In contrast, the syntectonic granites are compositionally variable with a spectrum between locally derived peraluminous, S-types (e.g. the Victor Harbor granite) through to obvious I-types, such as the Reedy Creek granodiorite, which are relatively calcic, hornblende-rich, and K_2O-poor (Figure 4). In comparison with the post-tectonic suite, they are Sr-rich with low Rb/Sr ratios, poorer in Y, Nb and Zr and have lower Nb/Zr ratios. They have low F abundances, and feldspar and biotite compositions which imply relatively high aH_2O. The apparent onset of the fractionation of zircon and accessory phases at SiO_2 contents < 70% implies evolution at temperatures lower than the post-tectonic series. These geochemical distinctions between the two suites are highlighted by the standard discrimination diagrams (Figure 5). For example on the Pearce *et al.* (1984) discrimination diagrams the early series with lower Rb and Y and Nb, fall in the volcanic-arc

Table 1 Analyses of Rathjen Gneiss samples and means of analyses of syntectonic (45 samples) and post-tectonic (36 samples) granites from the southern Adelaide Fold-Thrust Belt.

	88-RG1 Rathjen	898-309 Rathjen	Syntectonic	SD	Post-tectonic	SD	Syntectonic S-type	SD
SiO_2	73.67	73.97	68.8	4.3	72.0	7.5	72.1	1.2
TiO_2	0.55	0.44	0.6	0.2	0.4	0.5	0.5	0.1
Al_2O_3	12.26	12.45	14.8	1.7	13.5	1.9	13.4	0.9
Fe_2O_3*	3.39	2.81	3.7	1.2	2.7	2.3	3.4	0.3
MnO	0.04	0.03	0.0	0.0	0.0	0.0	0.1	0.0
MgO	0.9	0.81	1.3	0.7	0.6	1.2	1.5	0.2
CaO	1.7	1.66	2.6	1.1	1.6	2.2	1.6	0.2
Na_2O	3.41	3.55	3.7	0.7	3.8	0.4	2.6	0.2
K_2O	3.23	3.17	3.4	0.9	4.4	1.5	3.8	0.5
P_2O_5	0.11	0.44	0.1	0.1	0.1	0.1	0.1	0.1
Total	99.52	99.33	99.6	0.3	99.6	0.3	99.5	0.3
Al index	1.01	1.01	1.03	0.04	0.98	0.06	1.18	0.05
Mg#	0.34	0.37	0.39	0.07	0.21	0.14	0.47	0.01
K_2O/Na_2O	0.95	0.89	1.02	0.53	1.19	0.45	1.48	0.19
Cr	4	4	26	13	5	1	63	17
Ni	10	7	9	6	6	8	15	11
Sc	9.5	8.7	9	4	7	6	12	2
V	47	40	77	61	29	62	55	9
Rb	132.19	123	138	49	146	73	190	40
Sr	110.34	115	303	200	158	259	147	9
Ba	664	697	935	545	371	189	547	48
Ga	18	16	19	2	19	2	17	3
Y	62	41	33	23	58	35	38	16
Zr	314	260	246	69	231	89	167	20
Nb	16.4	13	15	2	23	6	15	1
La	68	48	55	20	72	45	29	3
Ce	137	102	98	40	134	82	59	10
Nd	56.89	42	39.4	18.6	51.8	32.7	24.3	13.3
Sm	10.99	–	7.0	3.8	9.7	6.1	5.2	2.6
Zr/Nb	19.1	20.0	16.0	3.4	10.6	4.4	11.6	2.2
Y/Nb	3.8	3.2	2.1	1.3	2.6	1.4	2.9	1.2
Zr/Y	5.1	6.3	0.4	0.4	4.9	2.7	1.6	2.5
La/Y	1.1	1.2	3.3	4.2	1.6	1.3	0.9	0.3
$^{143}Nd/^{144}Nd$ (t = 0)	0.512052 ± 25	–	0.512128	0.000140	0.512319	0.000127	0.511829	0.00013
$^{143}Nd/^{144}Nd$(t = 500)	0.511657	–	0.511792	0.000189	0.511949	0.000085	0.511384	0.00011
$^{147}Sm/^{144}Nd$	0.1169	–	0.1055	0.0192	0.1161	0.0192	0.1310	0.0073
ϵ Nd(t = 0)	–11.43	–	–9.9	2.7	–6.2	2.5	–15.7	2.7
ϵ Nd(I)	–6.2		–4.1	3.5	–1.2	1.7	–11.4	2.1
Model Age (DM)	1.6	–	1.4	0.4	1.2	0.2	2.3	0.1
$^{87}Sr/^{86}Sr$ (t = 0)	0.73701	–	0.72784	0.02058	0.76842	0.05730	0.74435	0.00323
$^{87}Sr/^{86}Sr$(I)	0.71144		0.70921	0.00409	0.70386	0.00097	0.71873	0.00108
$^{87}Rb/^{86}Sr$	3.48		2.6	2.4	9.3	8.4	3.5	0.6

All data quoted to 2σ.

granites field, while the later series are all in the within-plate granites field (Figure 5).

The two granite groups also have distinctive Nd and Sr isotopic compositions (Figures 6, 7). The younger suite has limited variation of isotopic compositions and quite primitive (non-crustal) compositions. Initial ϵ_{Nd} values are in the range -2 to +2 and $^{87}Sr/^{86}Sr_{(I)}$ values are in the range 0.7045–0.7065 (Turner *et al.* 1992). By comparison the older suite shows much more variable isotopic composition with $\epsilon_{Nd(I)}$ ranging from −13 to +1 and $^{87}Sr/^{86}Sr_{(I)}$ from 0.7050 to 0.7250. We interpret these geochemical signatures to indicate that the post-tectonic suite is dominated by mantle sources (Turner *et al.* 1992; Turner 1996; Turner & Foden 1996) whereas the syntectonic suite has a more significant crustal component.

FIELD SETTING AND GEOCHEMISTRY OF THE RATHJEN GNEISS

The Rathjen Gneiss is a coarse- to medium-grained orthogneiss of granitic to granodioritic composition with 'I-type' mineralogy and chemistry. It is composed of quartz, partly zoned plagioclase ($An_{25–45}$) and mildly perthitic microcline. The main ferromagnesian mineral is biotite,

but hornblende is also common. Minor or accessory phases include apatite, zircon, sphene, magnetite and rare allanite. In outcrop it forms a sheet-like structure in the core of a regional north-northwest-trending anticline, exposed in elevated country to the south of Springton. The main body of the Rathjen Gneiss forms a narrow canoe-shaped body, up to 3 km wide and 12 km long between Springton and the Tungkillo–Palmer road (Figure 2). A thin 'tail' about 100 m wide extends further southwards for another 8 km. Both the main body and the tail are essentially concordant with the regional stratigraphy, hosted by migmatitic metasediments of the Backstairs Passage Formation of the Kanmantoo Group. The outcrop pattern is consistent with the Rathjen Gneiss forming a sheet-like body several hundred metres thick. This concordance has led a number of authors (e.g. Fleming & White 1984) to argue that the Rathjen Gneiss is derived from a volcanic succession. However, recent gullying near the northern end of the granite (Adelaide 1:250 000 map sheet, GR 210000E, 710500N), has exposed clear intrusive contacts between narrow granite apophyses and the surrounding metasediments (Figures 2, 3). Likewise, near the southern 'tail', thin layers of felsic magmatic rock outcrop as discontinuous horizons parallel to the bedding of host Kanmantoo Group metasediments beneath the Rathjen Gneiss. In the past these have been taken as evidence for a synsedimentary volcanic origin; however, it is clear that this interpretation is not justified as mildly discordant apophyses, which contain metasedimentary xenoliths, also intrude from the upper surface of the sill into the overlying metasedimentary rocks (Figure 3).

Although the overall concordant nature and sheet-like geometry of the body in part reflect an original sill-like emplacement, this shape also reflects strain associated with the development of the prominent gneissosity, which is essentially parallel to the surrounding stratigraphy and to the migmatitic layering developed in the surrounding metasediments. The tectonic significance of this foliation remains obscure. It is largely confined to the immediate environment of the syntectonic granites between Murray Bridge and Springton becoming much less prominent in the lower grade rocks to the north. The foliation is associated

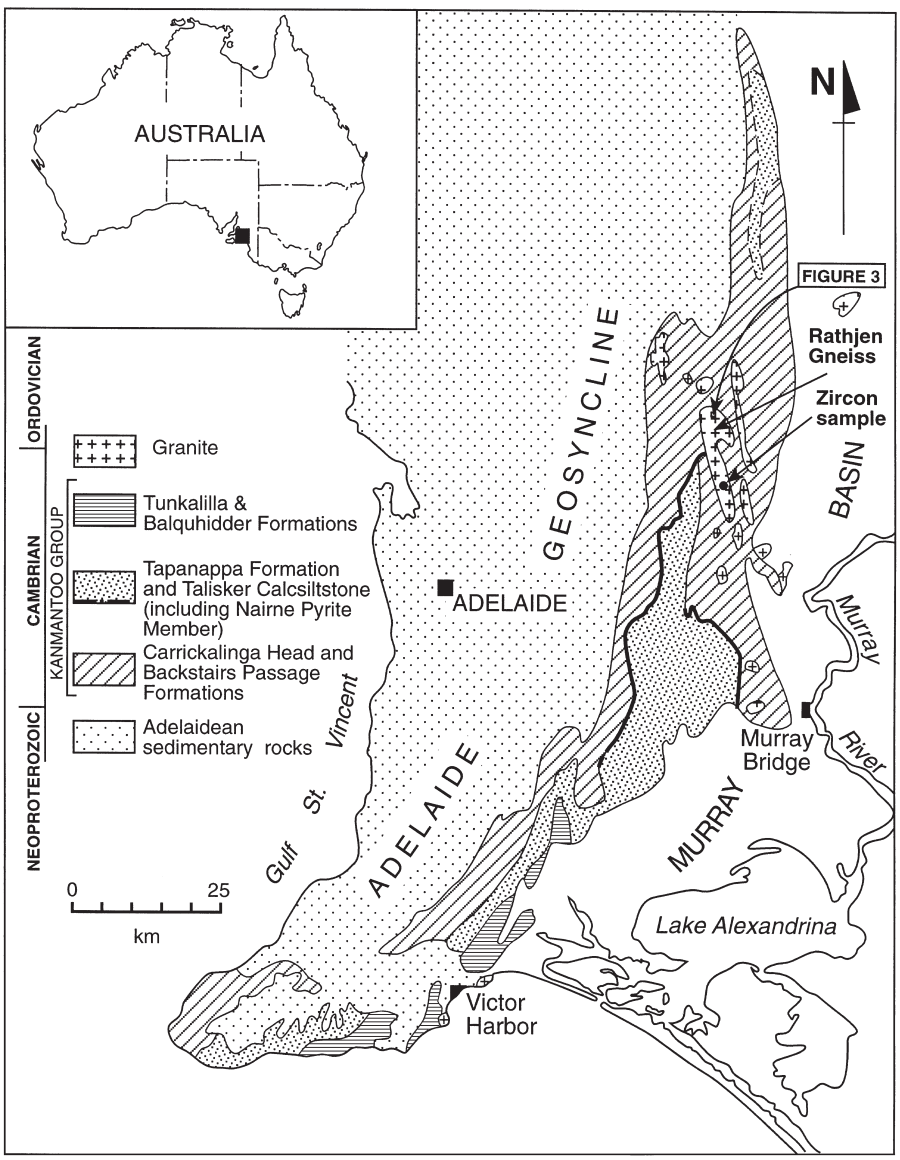

Figure 2 Southern Adelaide Geosyncline area showing principal granites of the syntectonic suite, including the Rathjen Gneiss. The sample site and the location of Figure 3 are indicated.

with north–south-trending lineations in part formed by its intersection by younger axial-plane fabrics to upright second-generation folds. However, as discussed by Oliver and Zakowski (1995) this north–south lineation is, in some places, demonstrably a mineral-elongation lineation and therefore implies a strain increment with a principal north–south stretch direction during the associated deformation. This direction is orthogonal to the principal convergence direction associated with development of younger (second generation) regional-scale folds in this part of the belt. Oliver and Zakowski (1995) attributed this north–south stretching to a period of previously unrecognised regional extensional deformation in the orogenic belt.

In the context of the regional geochemical variation of the granites, the Rathjen Gneiss is distinctive (Table 1). Although clearly the earliest of the syntectonic suites it has geochemical and isotopic characteristics transitional between the syntectonic and post-tectonic suites, as indicated by relatively high rare-earth elements, high Zr, Nb and Y and high Nb/Zr ratios. On the Rb *vs* Nb+Y and Y *vs* Nb discrimination diagrams it lies directly on the transition between the volcanic-arc granites and within-plate granites fields (Figure 5) and on all other geochemical variation diagrams falls between the syn- and post-tectonic fields (Figures 4–7). Ce or Zr *vs* SiO_2 variation typifies the contrasting evolution of the syn- and post-tectonic series. Whereas the post-tectonic suite shows enrichment of REE and Zr to SiO_2 levels > 70%, the syntectonic suite shows depletion of these elements when SiO_2 exceeds 70%. This behaviour is controlled by the later onset of accessory phase (apatite, zircon, allanite) saturation in the post-tectonic suites. In keeping with its transitional behaviour for other elements, on Harker diagrams the Rathjen Gneiss plots directly where the two series diverge.

As with other geochemical parameters, the Rathjen Gneiss also has transitional isotopic compositions, with ϵ_{Nd} −6 and $^{87}Sr/^{86}Sr_{(I)}$ of 0.7100 (Figures 6, 7; Table 1). It should also be noted that the initial Nd and Sr isotopic compositions of the Rathjen Gneiss are significantly different from either the host Kanmantoo Group metasediments ($\epsilon_{Nd}] = -13$, $^{87}Sr/^{86}Sr_{(I)} = 0.7250$) or possible Proterozoic crystalline basement at depth ($\epsilon_{Nd} < -20$, $^{87}Sr/^{86}Sr > 0.7550$) at 514 Ma. The isotopic composition of the Rathjen Gneiss lies on a continuum of Nd and Sr isotopic variation between mantle and crustal sources defined by the granites that form the syntectonic suite.

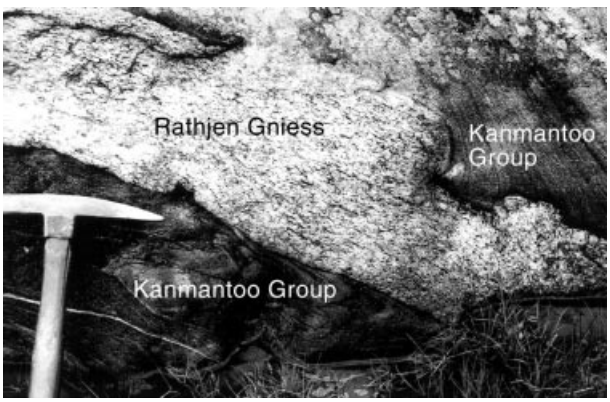

Figure 3 Intrusive contacts between apophyses of the Rathjen Gneiss and the surrounding metasediments at location GR 210000E, 710500N. See Figure 2 for location.

AGE OF THE RATHJEN GNEISS

In order to assess the age of emplacement of the Rathjen Gneiss and thus a maximum age of initiation of the Delamerian Orogeny we have separated zircons and carried out U–Pb isotopic analysis both by ion probe (SHRIMP I and II) at the Research School of Earth Sciences, Australian National University and the emitter bedding Pb–Pb technique (Kober 1987) at the University of Adelaide (Dougherty-Page & Foden 1996). In both cases we have used

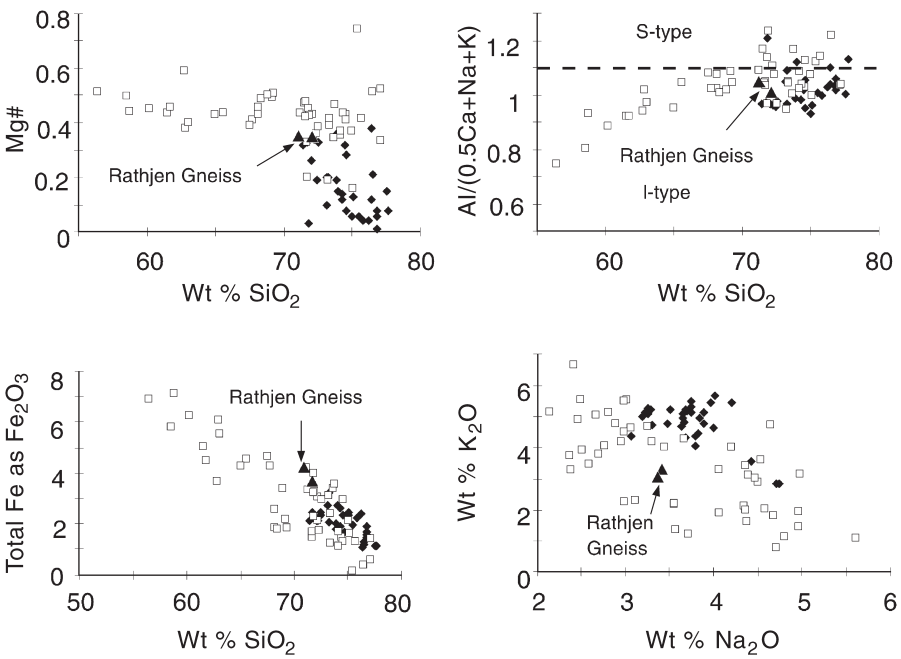

Figure 4 Major element composition of Cambro-Ordovician granites from the Adelaide Fold-Thrust Belt. □, syn-Delamerian granites; ◆, post-Delamerian granites; ▲, Rathjen Gneiss.

zircons from the same population that were separated from 10 kg of crushed sample from the southern end of the main Rathjen Gneiss body (Figure 2: Adelaide 1:250 000 map sheet, GR 214550E, 698550N). The zircons were examined optically and using cathodoluminescence (Koschek 1993) and were found to have a complex structure (Figure 8). The grains were typically medium sized, (150–200 μm) and were short, prismatic, doubly terminated euhedra, unlike the elongate forms commonly associated with precipitation from felsic volcanic magmas. Under cathodoluminescence a large proportion of grains have a three-fold structure consisting of a variable sized rounded core, surrounded by a broad layer of euhedrally zoned zircon and, finally, a thin (< 10 μm thick) structureless outer zone. SHRIMP ion probe analyses revealed that the cores were older (inherited) and in general relatively U-rich. The euhedrally zoned layer has moderate to low U content and high Th/U ratios, clearly implying a magmatic origin. The thin outermost zones are U-rich and most have very low Th/U ratios and are the probable products of growth from a metamorphic fluid or from a hydrous minimum melt.

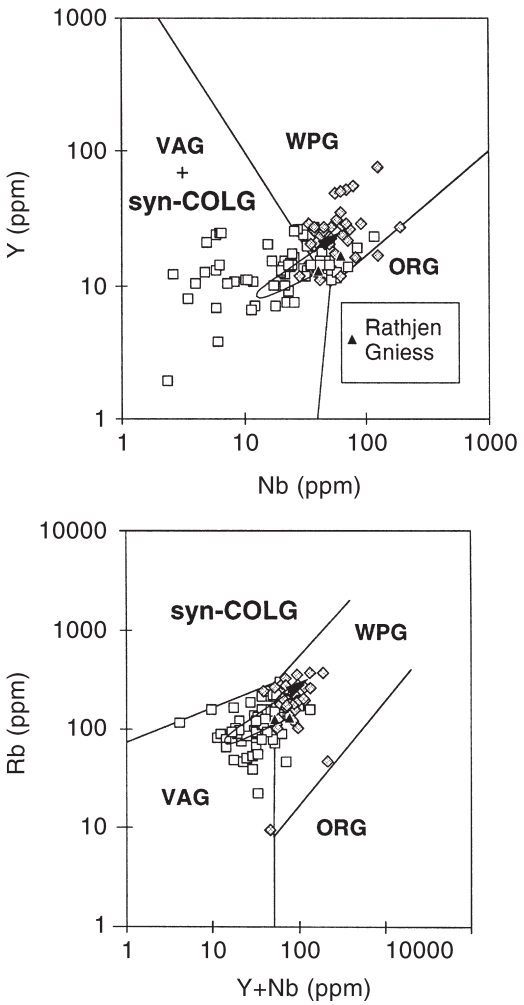

Figure 5 Geochemical discrimination diagrams of Pearce *et al.* (1984). □, syn-Delamerian granites; ◇, post-Delamerian granites; ▲, Rathjen Gneiss. Arrow indicates the general temporal shift of granite composition from earliest Delamerian to post-Delamerian. VAG, volcanic-arc granites; syn-COLG, syn-collisional granites; WPG, within-plate granites; ORG, oceanic granites.

Zircon evaporation ('Kober' technique) data

In the 'Kober' technique individual zircon crystals were crimped into Re filaments, and heated in a Finnigan Mat 261 mass spectrometer. Pb-isotope ratios were determined dynamically, using a Secondary Electron Multiplier set at constant amplification, scanning in the order 206 – 207 – 208 – 207 – 206 – 204. Heating the zircon results in the breakdown of zircon to baddeleyite (ZrO_2) (Chapman & Roddick 1994), releasing radiogenic Pb, from which an age is determined. Within a high-quality crystal, the breakdown takes place along a sharply defined reaction front, which progresses into the grain with continued heating. Depending on age and U content an individual zircon crystal may contain sufficient Pb for several analyses in which case it may be analysed in a series of discrete heating steps.

The $^{207}Pb/^{206}Pb$ age given by each heating step represents the average age of radiogenic lead released by the passage of the reaction front through the crystal during that step. Thus the $^{207}Pb/^{206}Pb$ age only represents a true crystallisation age when this material is a single isotopically concor-

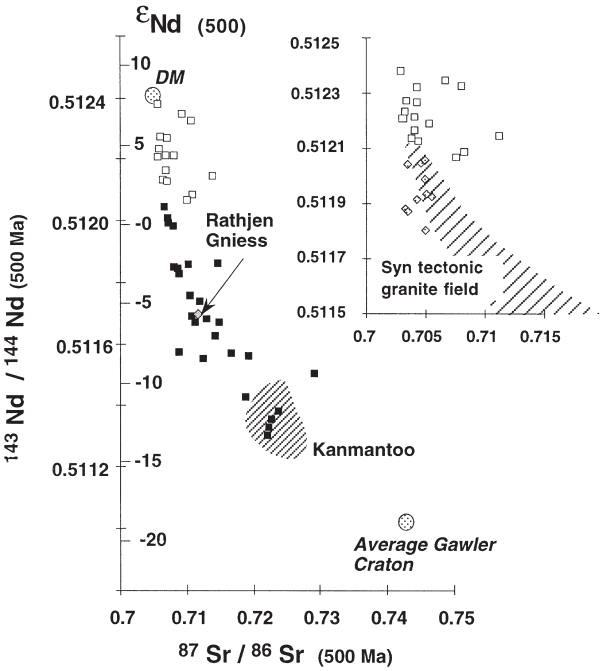

Figure 6 Initial (500 Ma) Nd–Sr isotopic composition of Cambro-Ordovician magmatic rocks from the Adelaide Fold-Thrust Belt. □, mafic rocks; ■, syn-Delamerian granites. Rathjen Gneiss indicated. The inset shows the post-Delamerian granites (◇) and the Delamerian mafic rocks (□) and the upper part of the syntectonic field shaded. DM, depleted mantle at 500 Ma. The Gawler Craton mean is that of Palaeoproterozoic to Mesoproterozoic basement rocks from the craton to the west of the Adelaide Fold-Thrust Belt. The shaded Kanmantoo field is that of Cambrian clastic sedimentary rocks which are intruded by the Cambrian granites (data source Turner *et al.* 1992 and authors' unpubl. data).

dant phase of zircon. The passage of the reaction front through several isotopically distinct domains results in a geologically meaningless 'mixed age' proportional to the relative quantities of Pb supplied by each of the end-member components. Thus incorporation of material derived from a later rim results in an age younger than the true crystallisation age, while the incorporation of material derived from an inherited core results in an age older than the true crystallisation age for that heating step. A distinct age plateau, reproduced by several heating steps, strongly indicates a true concordant crystallisation age as it is considered unlikely that several distinct age components will repeatedly mix in the same proportions. In this study, zircons with radiation damage, large cracks or obvious cores were avoided as the reaction front propagates rapidly along cracks and through radiation damaged areas. Such damage to a crystal increases total area of the reaction front within the zircon crystal and thus decreases the possible resolution of zonation.

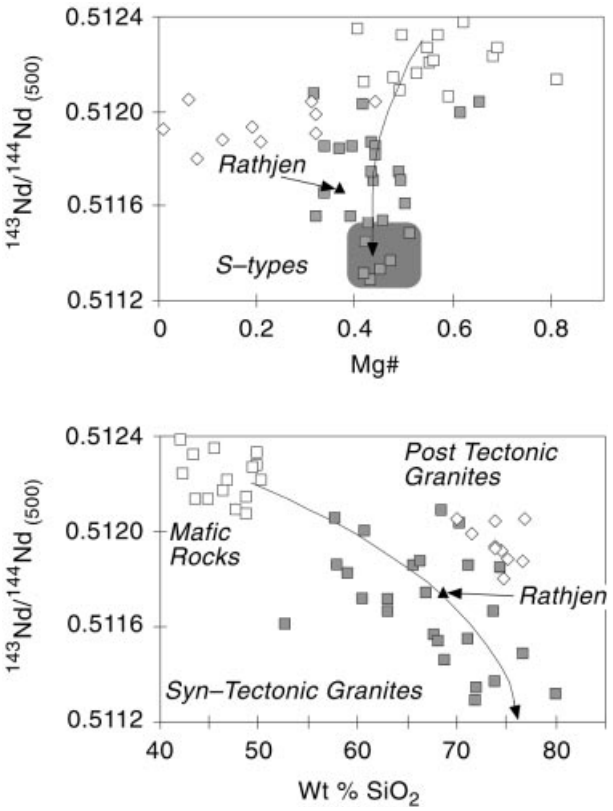

Figure 7 SiO_2 and Mg# *vs* initial Nd isotopic composition. □, Delamerian mafic rocks; ■, syn-Delamerian granites; ◇, post-Delamerian granites. Rathjen Gneiss indicated. S-types field is that of samples with Al index (see Figure 4) > 1.1. Arrow illustrates a possible contemporary mantle–crust mixing trend to explain the source of the syntectonic granites.

Ages given by step-heating data for Rathjen Gneiss zircons (Table 2) were sorted in order of ascending age and each data point was then assigned a rank within this sorted sequence (with the youngest analysis given a rank of 1). Heating steps are then plotted as their age against rank (Figure 9). In this graph, mixing between various age components results in inter-step age variation while true ages tend to be more frequently repeated, producing distinct age plateaux. This type of graph has advantages over the frequency histograms traditionally used to present zircon evaporation data (Kober 1987; Dougherty-Page & Foden 1996) in that the degree of complexity within the population is immediately apparent, the visual interpretation of age plateau does not depend on arbitrary bin sizes, and each individual data point may be identified and its associated analytical error displayed.

The addition of non-radiogenic ^{207}Pb derived from common Pb results in an overestimation of the $^{207}Pb/^{206}Pb$ age. The effect of common Pb addition is greater in

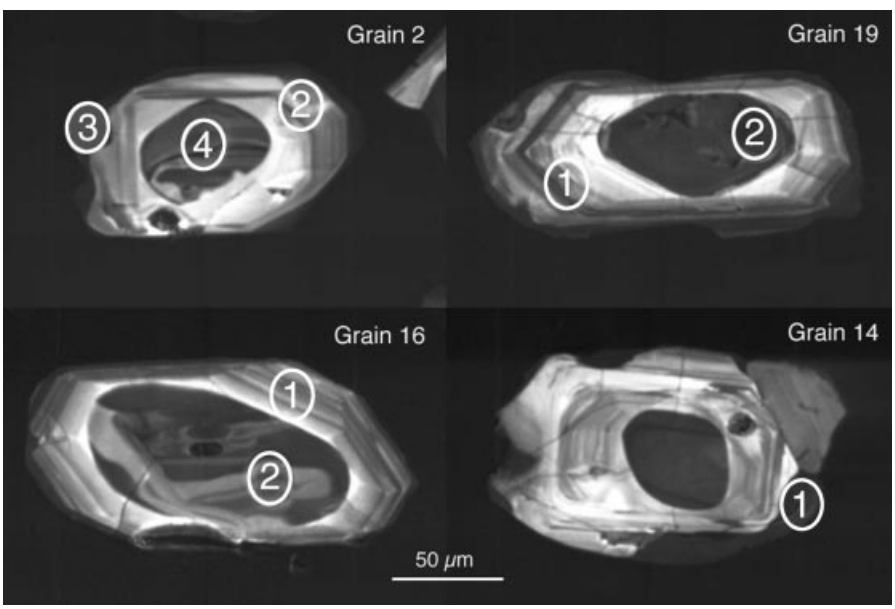

Figure 8 Cathodoluminescence–SEM images of zircons from the Rathjen Gneiss. Circled numbers refer to analysis spots as given in Table 3. The grains show the 3-fold growth structure common to most zircon from the gneiss: (i) a rounded non-luminescent core that isotopic analysis reveal to be inherited; (ii) a sequence of moderately luminescent euhedral growth zones interpreted as magmatic in origin; and (iii) an irregular structureless non-luminescent rim interpreted as subsolidus or near-solidus growth during subsequent high-grade metamorphism (note the irregular overgrowth abutting the grey feldspar grain adhering to the upper right corner of grain 14). In grain 14 the embayed boundary between the zoned zircon and overgrowth suggests a period of zircon dissolution between the magma crystallisation and the subsequent metamorphism.

Table 2 Pb isotope data for analysis of 16 zircons from the Rathjen Gneiss in a total of 32 heating steps (plotted on Figure 9).

Zircon	Step	$^{208}Pb/^{206}Pb$	$^{207}Pb/^{206}Pb$	$^{204}Pb/^{206}Pb$	Age	Rank
1	1	0.121327 ± 0.011082	0.057819 ± 0.000227	bd	520 ± 8	13
1	2	0.26708 ± 0.003405	0.058352 ± 0.000505	bd	540 ± 6	19
1	3	0.410837 ± 0.025158	0.057863 ± 0.000638	bd	521 ± 15	15
1	4	0.488448 ± 0.002832	0.057767 ± 0.000123	bd	518 ± 6	11
2	1	0.368267 ± 0.003109	0.057784 ± 0.000202	bd	518 ± 7	12
2	2	0.406225 ± 0.001355	0.057762 ± 0.000495	bd	517 ± 13	10
3	1	0.110689 ± 0.005675	0.057598 ± 0.000257	bd	511 ± 8	7
3	2	0.161385 ± 0.005008	0.059198 ± 0.000156	bd	571 ± 6	21
3	3	0.047041 ± 0.000001	0.066455 ± 0.000185	bd	819 ± 6	26
5	1	0.132161 ± 0.00048	0.059172 ± 0.000354	bd	570 ± 10	20
5	2	0.133235 ± 0.002513	0.06539 ± 0.000057	bd	785 ± 4	24
5	3	0.113863 ± 0.000706	0.069226 ± 0.000408	bd	904 ± 9	27
6	1	0.156016 ± 0.001634	0.079439 ± 0.003441	bd	1182 ± 45	29
6	2	0.117308 ± 0.256358	0.129834 ± 0.001246	bd	2095 ± 10	30
6	3	0.067176 ± 0.000032	0.147628 ± 0.00026	bd	2318 ± 3	31
6	4	0.066245 ± 0.000158	0.154921 ± 0.00011	bd	2401 ± 2	32
7	1	0.141948 ± 0.005028	0.057663 ± 0.000036	bd	514 ± 4	8
7	2	0.24483 ± 0.00056	0.057909 ± 0.000287	bd	523 ± 9	17
8	1	0.198362 ± 0.00192	0.061899 ± 0.000399	0.000043 ± 0.00002	649 ±	22
9	1	0.222855 ± 0.125824	0.057861 ± 0.00055	bd	521 ± 14	14
10	1	0.381454 ± 0.002066	0.057435 ± 0.000029	bd	505 ± 4	2
10	2	0.43371 ± 0.000774	0.057538 ± 0.000113	bd	509 ± 6	5
11	1	0.12652 ± 0.017104	0.063655 ± 0.001678	0.000067 ± 0.000028	698 ±	23
11	2	0.19477 ± 0.000764	0.070656 ± 0.000028	bd	946 ± 3	28
12	1	0.15467 ± 0.003154	0.057672 ± 0.000086	bd	514 ± 5	9
12	2	0.303685 ± 0.002811	0.058398 ± 0.000043	0.000067 ± 0.000053	507 ±	3
14	1	0.128751 ± 0.010232	0.057506 ± 0.000124	bd	508 ± 6	4
14	2	0.243935 ± 0.006716	0.057409 ± 0.000034	bd	504 ± 4	1
14	3	0.189724 ± 0.005222	0.057578 ± 0.000647	bd	510 ± 16	6
15	1	0.126444 ± 0.000617	0.065926 ± 0.003711	bd	802 ± 61	25
16	1	0.135434 ± 0.002	0.057866 ± 0.000677	bd	521 ± 16	16
16	2	0.039772 ± 0.094947	0.058016 ± 0.000119	bd	527 ± 6	18

bd, below detection.
Isotope ratios are uncorrected for common Pb, all errors are quoted to 2σ. Where $^{204}Pb/^{206}Pb$ was below detection, a ratio of 0.000005 ± 0.000005 (2σ) was applied in the common Pb age correction (see text for discussion). The rank of the heating steps refers to their relative positions when tabulated in ascending order of common Pb corrected age, with the youngest ranked 1 and the oldest 32.

comparatively recent rocks such as the Rathjen Gneiss than in more ancient samples, due to the decrease in the production of radiogenic ^{207}Pb relative to radiogenic ^{206}Pb through time. Common Pb contents are determined from $^{204}Pb/^{206}Pb$ ratios and corrected by application of the equation suggested by Cocherie *et al.* (1992). The appropriate common Pb isotopic composition for the age of the zircon was determined from the Stacey and Kramers (1975) two-stage Pb-evolution curve. As a consequence of a dynamic collection routine in which all Pb-isotope beams were measured at constant amplification, the smaller ^{204}Pb beam was frequently below detection. Quoted crystallisation ages are calculated from the average age of the plateau heating steps which record a single zircon growth stage. Errors quoted on age estimations are 2σ (excluding individual analytical errors). Where age estimations are based on assumed values of common Pb, the effect of the assumed correction (±3 Ma at 500 Ma) is added to the quoted error. During the analyses of zircons from the Rathjen Gneiss, zircons from the Palaeoproterozoic Coulta Granodiorite, used as a standard at the University of Adelaide, were also analysed. They returned an age of 2512 ± 2 Ma (2σ, weighted average), against an internally accepted value of 2514 ± 7 Ma, and an external (SHRIMP) determination of 2520 ± 9 Ma (C. M. Fanning pers. comm. 1997).

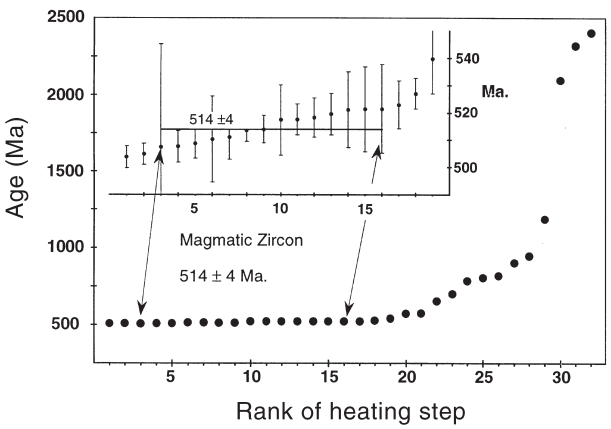

Figure 9 Common Pb corrected age data computed from $^{207}Pb/^{206}Pb$ measurements on 32 heating steps carried out on zircons from the Rathjen Gneiss (data in Table 2). The ages given by these heating steps have been sorted into ascending order and are plotted against their 'rank' within this age sequence. The main diagram shows a clear lower age plateau at *ca* 500 Ma, with older ages due to inheritance becoming predominant after heating step rank number 17. The inset shows the plateau on an expanded scale, with 2σ error bars on the individual heating steps. The 14 steps indicated between the arrows yield an age of 514 ± 4 Ma.

Fourteen zircon crystals were analysed, in a total of 32 heating steps. Eight of these zircons contained inherited cores. No distinct age plateau were achieved for these inherited zircon heating steps and oldest ages recorded from individual inherited zircon grains are regarded as minimum ages for that core, as the final analysis may still have contained a component of zircon of Rathjen Gneiss magmatic age. Excluding the heating steps of very variable age from rank 17 onwards (taken to be inherited cores) and the first two ranked steps, the age of magmatic zircon growth is interpreted as given by the 14 heating steps from ranks 3 to 16 inclusive (Figure 9). This plateau is formed by a continuous suite of ages from 507 to 521 Ma. and yields a crystallisation age of the Rathjen Gneiss of 514 ± 4 Ma (2σ, including error due to estimated common Pb correction). This age is identical to that achieved with the SHRIMP by analysis of the broad, euhedrally zoned areas of the zircons (see below). As it was clear from the cathodoluminescence images that the zircons had a complex internal history, ion microprobe analyses were undertaken to assess to what extent the Pb–Pb evaporation ages were influenced by older Pb from the inherited cores, or from possible younger Pb in the thin outermost rims.

Ion microprobe (SHRIMP) data

Preliminary ion probe results were initially obtained using SHRIMP I and were subsequently repeated using SHRIMP II. Analysis techniques were similar to those used by Williams and Claesson (1987). Although the two SHRIMP analysis sessions yielded consistent results, the earlier session was completed before the zonal structure of the zircons was recognised. Therefore SHRIMP results in Table 3 include data from inherited cores from both sessions, but only that from the SHRIMP II sessions for magmatic euhedrally zoned zircon and the thin overgrowths (Figure 10).

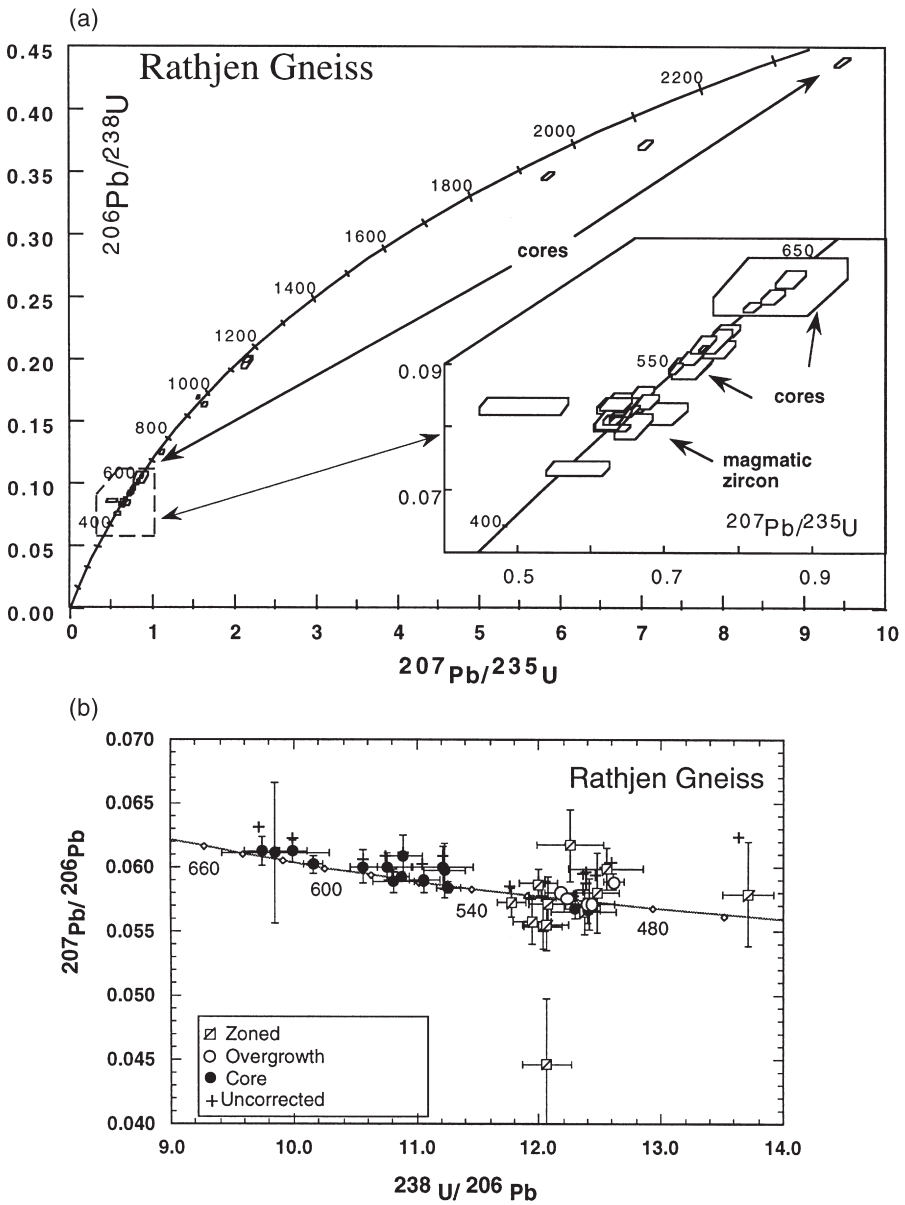

Figure 10 (a.) Concordia plot of SHRIMP U–Pb isotopic analyses (data in Table 3). The enlargement highlights magmatic zircon populations and Late Neoproterozoic inherited cores with ages ranging from 650 to 550 Ma. (b.) $^{207}Pb/^{206}Pb$ *vs* $^{238}U/^{206}Pb$ (Tera-Wasserburg) diagram. Crosses indicate analyses before common Pb correction. Squares with diagonal lines represent analyses of the broad euhedrally zoned magmatic rims (luminescent zone in the cathodoluminescence image in Figure 8), yielding an age of 514.6 ± 5.9 Ma (2σ). Open circles are thin metamorphic overgrowths [503.3 ± 7.4 Ma (2σ)]. Filled circles are analyses from cores.

Table 3 Pb and U isotopic data and age calculations from the SHRIMP analyses of zircons from the Rathjen Gneiss (plotted in Figure 10).

	U ppm	Th ppm	Th/U	Pb* ppm	$^{204}Pb/^{206}Pb$	%206 com.	$^{208}Pb/^{206}Pb$	$^{208}Pb/^{232}Th$	$^{206}Pb/^{238}U$	$^{207}Pb/^{235}U$	$^{207}Pb/^{206}Pb$	Age 8/32	Age 6/38	Age 7/35	Age 7/6
Overgrowth															
20.1	1648	66	0.04	124	0.000016	0.03	0.0105 ± 0.0005	0.0215 ± 0.001	0.0818 ± 0.0006	0.651 ± 0.007	0.0577 ± 0.0004	430 ± 20	507 ± 3	509 ± 4	518 ± 14
21.1	1044	769	0.74	78	0.000121	0.19	0.0205 ± 0.001	0.0022 ± 0.001	0.0806 ± 0.0006	0.633 ± 0.008	0.057 ± 0.0006	45 ± 2	500 ± 4	498 ± 5	492 ± 22
14.1	950	915	0.96	70	0.000103	0.16	0.0272 ± 0.0012	0.0022 ± 0.001	0.0793 ± 0.0005	0.644 ± 0.008	0.0589 ± 0.0006	45 ± 2	492 ± 3	505 ± 5	564 ± 23
2.3	930	52	0.06	71	0.000003	0	0.0177 ± 0.0005	0.0259 ± 0.0008	0.0821 ± 0.0009	0.657 ± 0.009	0.058 ± 0.0004	517 ± 15	509 ± 5	513 ± 6	530 ± 16
15.1	911	37	0.04	67	0.000089	0.14	0.091 ± 0.0011	0.018 ± 0.0022	0.0808 ± 0.0006	0.635 ± 0.009	0.057 ± 0.0006	360 ± 44	501 ± 3	499 ± 6	491 ± 25
Zoned															
17.1	334	394	1.18	35	0.000083	0.13	0.3555 ± 0.0032	0.0256 ± 0.0004	0.0849 ± 0.0009	0.671 ± 0.016	0.0573 ± 0.0012	511 ± 7	525 ± 5	521 ± 10	503 ± 45
19.1	242	223	0.92	23	0.000115	0.19	0.2804 ± 0.0057	0.0252 ± 0.0006	0.0829 ± 0.001	0.653 ± 0.026	0.0572 ± 0.0021	503 ± 12	513 ± 6	511 ± 16	499 ± 82
16.1	169	148	0.87	16	0.000156	0.25	0.2528 ± 0.0056	0.024 ± 0.0007	0.083 ± 0.0013	0.635 ± 0.027	0.0555 ± 0.0021	479 ± 13	514 ± 8	499 ± 17	434 ± 86
25.1	158	167	1.06	15	0.00017	0.27	0.3267 ± 0.0061	0.0249 ± 0.0006	0.0806 ± 0.0013	0.635 ± 0.026	0.0571 ± 0.0021	497 ± 13	499 ± 8	499 ± 16	497 ± 81
18.1	129	119	0.92	12	0.00001	0.02	0.2826 ± 0.0043	0.0255 ± 0.0005	0.0834 ± 0.0011	0.675 ± 0.017	0.0587 ± 0.0012	509 ± 11	516 ± 6	524 ± 10	558 ± 43
23.1	129	101	0.78	12	0.000126	0.2	0.2432 ± 0.0049	0.0261 ± 0.0007	0.0838 ± 0.0011	0.644 ± 0.023	0.0558 ± 0.0018	520 ± 13	518 ± 6	505 ± 14	444 ± 72
15.2	122	262	2.14	11	0.000308	0.49	0.4051 ± 0.0103	0.0138 ± 0.0004	0.0729 ± 0.0011	0.583 ± 0.043	0.0579 ± 0.0041	277 ± 8	454 ± 7	466 ± 28	527 ± 162
32.1	110	130	1.18	11	0.000217	0.35	0.3556 ± 0.0049	0.0249 ± 0.0005	0.0831 ± 0.0011	0.634 ± 0.022	0.0554 ± 0.0017	498 ± 10	515 ± 6	499 ± 14	427 ± 71
8.2	91	74	0.82	8	0.00001	0.02	0.2616 ± 0.0049	0.0259 ± 0.0008	0.0809 ± 0.0017	0.63 ± 0.025	0.0565 ± 0.0018	516 ± 16	501 ± 10	496 ± 16	473 ± 71
24.1	78	76	0.98	7	0.00001	0.02	0.3123 ± 0.0058	0.0255 ± 0.0009	0.0797 ± 0.0019	0.658 ± 0.025	0.0599 ± 0.0016	508 ± 17	494 ± 12	514 ± 16	601 ± 59
22.1	58	54	0.93	6	0.00001	0.02	0.296 ± 0.0076	0.026 ± 0.0009	0.0816 ± 0.0018	0.694 ± 0.037	0.0617 ± 0.0028	519 ± 18	506 ± 11	535 ± 22	664 ± 101
Core															
28.1	2073	1803	0.87	217	0.000001	0	0.2624 ± 0.0011	0.0277 ± 0.0002	0.0919 ± 0.0005	0.752 ± 0.006	0.0593 ± 0.0003	553 ± 4	567 ± 3	569 ± 4	577 ± 12
40.1	1159	364	0.31	106	0.000072	0.12	0.0064 ± 0.0016	0.0021 ± 0.0005	0.1 ± 0.0011	0.845 ± 0.016	0.0613 ± 0.0009	41 ± 10	615 ± 7	622 ± 9	648 ± 30
11.2	1136	82	0.07	103	0.000013	0.02	0.0073 ± 0.0006	0.0099 ± 0.0008	0.0984 ± 0.0008	0.817 ± 0.012	0.0602 ± 0.0007	199 ± 16	605 ± 4	606 ± 6	612 ± 24
31.1	1089	52	0.05	89	0.000008	0.01	0.0137 ± 0.0005	0.0256 ± 0.0009	0.0888 ± 0.0008	0.715 ± 0.009	0.0584 ± 0.0004	511 ± 18	549 ± 5	548 ± 5	545 ± 17
19.2	720	517	0.72	269	0.000043	0.07	0.0546 ± 0.0011	0.0276 ± 0.0006	0.3628 ± 0.0033	7.051 ± 0.09	0.1409 ± 0.0011	551 ± 12	1996 ± 16	2118 ± 11	2239 ± 14
35.1	698	86	0.12	109	0.000038	0.06	0.0353 ± 0.001	0.0468 ± 0.0014	0.1644 ± 0.0015	1.559 ± 0.026	0.0687 ± 0.0009	925 ± 28	981 ± 8	954 ± 10	891 ± 27
22.2	619	302	0.49	54	0.000062	0.1	0.0279 ± 0.0013	0.0053 ± 0.0003	0.093 ± 0.0018	0.77 ± 0.022	0.06 ± 0.0011	107 ± 7	573 ± 11	580 ± 13	605 ± 39
41.1	565	335	0.59	272	0.00001	0.02	0.1433 ± 0.0011	0.1037 ± 0.0013	0.4281 ± 0.0037	9.473 ± 0.099	0.1605 ± 0.0008	1994 ± 23	2297 ± 17	2385 ± 10	2461 ± 8
16.2	526	43	0.08	43	0.000078	0.12	0.0155 ± 0.0027	0.0168 ± 0.0029	0.0891 ± 0.0013	0.734 ± 0.03	0.0597 ± 0.0021	337 ± 58	550 ± 8	559 ± 18	593 ± 80
36.1	481	810	1.69	53	0.000128	0.2	0.1796 ± 0.003	0.011 ± 0.0011	0.1027 ± 0.0014	0.868 ± 0.021	0.0613 ± 0.0011	220 ± 23	630 ± 8	634 ± 11	649 ± 39
39.1	444	349	0.79	45	0.000082	0.13	0.2428 ± 0.0027	0.0279 ± 0.0005	0.0904 ± 0.001	0.736 ± 0.016	0.059 ± 0.001	557 ± 9	558 ± 6	560 ± 9	569 ± 38
10.2	357	409	1.15	44	0.000131	0.21	0.1053 ± 0.003	0.0112 ± 0.0003	0.1214 ± 0.0015	1.112 ± 0.028	0.0664 ± 0.0014	224 ± 7	739 ± 8	759 ± 14	820 ± 45
2.4	321	87	0.27	32	0.00001	0.02	0.095 ± 0.0113	0.0356 ± 0.0045	0.1015 ± 0.0046	0.856 ± 0.09	0.0611 ± 0.0055	707 ± 89	623 ± 27	628 ± 50	644 ± 206
38.1	282	584	2.07	48	0.000094	0.15	0.1601 ± 0.002	0.0123 ± 0.0002	0.1592 ± 0.0016	1.639 ± 0.032	0.0747 ± 0.0012	248 ± 4	953 ± 9	985 ± 13	1059 ± 32
34.1	273	319	1.17	32	0.000042	0.07	0.3569 ± 0.0038	0.0289 ± 0.0004	0.0946 ± 0.0009	0.784 ± 0.019	0.0601 ± 0.0013	576 ± 9	583 ± 6	588 ± 11	606 ± 46
42.1	270	175	0.65	100	0.000032	0.05	0.1451 ± 0.0018	0.0755 ± 0.0013	0.3383 ± 0.0036	5.847 ± 0.081	0.1253 ± 0.0009	1472 ± 25	1879 ± 18	1953 ± 12	2034 ± 13
8.3	243	445	1.83	30	0.00005	0.08	0.4836 ± 0.0068	0.0244 ± 0.0007	0.0925 ± 0.0015	0.752 ± 0.018	0.0589 ± 0.0009	488 ± 14	570 ± 9	569 ± 10	564 ± 35
37.1	179	132	0.74	18	0.000015	0.02	0.2034 ± 0.0048	0.0253 ± 0.0007	0.0918 ± 0.0013	0.771 ± 0.025	0.0609 ± 0.0016	504 ± 14	566 ± 8	580 ± 14	635 ± 60
33.1	171	242	1.42	36	0.000092	0.15	0.1914 ± 0.0032	0.0263 ± 0.0005	0.1944 ± 0.0021	2.156 ± 0.046	0.0804 ± 0.0014	524 ± 11	1145 ± 11	1167 ± 15	1207 ± 33
26.1	82	93	1.13	9	0.00001	0.02	0.3701 ± 0.0071	0.0293 ± 0.0009	0.0892 ± 0.002	0.737 ± 0.029	0.06 ± 0.0017	583 ± 18	551 ± 12	561 ± 17	602 ± 64
27.1	79	44	0.56	16	0.00001	0.02	0.1752 ± 0.0042	0.0598 ± 0.0022	0.1921 ± 0.0049	2.158 ± 0.071	0.0815 ± 0.0015	1174 ± 42	1133 ± 26	1167 ± 23	1233 ± 37
9.1[a]	83	97	1.168	9	0.00001	0.18	0.3659 ± 0.009	0.0276 ± 0.001	0.0882 ± 0.002	0.732 ± 0.042	0.0602 ± 0.003	551 ± 19	545 ± 12	558 ± 25	609 ± 112
11.1[a]	1177	30	0.025	105	0.000089	0.16	0.0074 ± 0.001	0.0289 ± 0.0043	0.0975 ± 0.0022	0.8 ± 0.02	0.0595 ± 0.0006	576 ± 85	600 ± 13	597 ± 11	586 ± 20
10.1[a]	137	86	0.622	18	0.000162	0.29	0.2308 ± 0.007	0.0437 ± 0.0016	0.1179 ± 0.0026	1.021 ± 0.05	0.0628 ± 0.0025	865 ± 32	718 ± 15	714 ± 25	702 ± 88
13.1[a]	354	975	2.757	110	0.000119	0.22	0.6035 ± 0.003	0.0469 ± 0.0011	0.2141 ± 0.0048	2.452 ± 0.06	0.083 ± 0.0007	926 ± 21	1251 ± 25	1258 ± 18	1270 ± 16

[a]denotes SHRIMP I analyses; all others SHRIMP II. Four analysed spots from the SHRIMP II session have been omitted from the table (2.2, 3.2, 29.1, 30.1) due to high common Pb or clear Pb-loss. All data quoted to 1σ. These data are available on request from the senior author.

The broad euhedrally zoned component of the zircons is interpreted as magmatic crystallisation at the time of intrusion of the Rathjen Gneiss protolith. This zircon has low to moderate U contents and quite high Th/U ratios (mean about 0.95). From 11 spot analyses of this material, the ion microprobe data yielded a $^{206}Pb/^{238}U$ age of 514.6 ± 5.9 Ma (95% confidence level) which is identical to the result from the Kober method.

The thin outermost rims were difficult to analyse as they were mostly narrower than the ion beam spot. These have consistently very high U (900–1600 ppm) and some (but not all) have very low Th. These rims probably crystallised during post-intrusive metamorphism or even incipient partial melting of the Rathjen Gneiss. It seems probable that these rims represent growth during subsequent upper amphibolite facies metamorphism (D_2 and D_3) (Offler & Fleming 1968; Fleming & White 1984; Sandiford *et al.* 1992; Chen & Lui 1996). The SHRIMP II data yield a weighted mean $^{206}Pb/^{238}U$ age of 503 ± 7 Ma (95% confidence level), consistent with constraints provided by the ages of younger syntectonic granites in the belt.

In retrospect, it is clear that our evaporation Pb–Pb analyses must represent Pb largely derived from the broad zoned magmatic growths and the two datasets are strongly corroborative. The young 'Kober' ages (step ranks 1 and 2, Table 2) excluded from the evaporation plateau (Figure 9) probably incorporate some Pb from the these thin outer zones. Likewise, when the SHRIMP data (Table 3) are considered, the indistinct upper limit of the magmatic zircon plateau (at step ranks 15–18) is likely to reflect the effects of mixed evaporation of magmatic and minor amounts of inherited zircon whose age is < 50 million years older than the age of crystallisation of the Rathjen Gneiss magma.

Age of inherited zircon cores

The combined age frequency spectrum of inherited core analyses from both SHRIMP I and II (Table 3) and from Pb–Pb evaporation results are plotted in Figure 11. These results show ages to be broadly clustered in the Neoproterozoic and in the Late Archaean and earliest Palaeoproterozoic. In detail there are suggestions of peaks in the range 675–550 Ma, *ca* 1100–900 Ma, *ca* 1250 Ma, *ca* 2200–1950 Ma and *ca* 2500 Ma. These frequencies are quite unlike those of nearby Proterozoic crystalline basement (Gawler Craton, Olary, Broken Hill) which are dominated by ages in the range 1900–1580 Ma (Foden 1996). The inheritance pattern corresponds well with detrital zircons from Kanmantoo Group sedimentary rocks (Figure 11) and is unlike the Adelaidean sedimentary rocks whose detrital zircon population is dominated by Palaeoproterozoic and Mesoproterozoic (1850–1550 Ma) zircons (Foden 1996; Ireland *et al.* 1998). Along with the Nd isotopic composition the inherited zircon component implies that the Rathjen Gneiss protolith was not sourced from typical Palaeoproterozoic to Mesoproterozoic South Australian cratonic basement.

ORIGIN OF THE RATHJEN GNEISS

The composition of the Rathjen Gneiss is transitional between that of the granites of the post-tectonic suite whose ages are in the range 490–480 Ma (Turner *et al.* 1992; Turner & Foden 1996) and that of the syntectonic suite (e.g. Cape Willoughby Granite, Kangaroo Island, 508±7 Ma: Fanning 1990). Because it has high Nb/Y and Nb/Rb ratios, the Rathjen Gneiss plots in the within-plate granites field on geochemical discrimination diagrams for granites (Pearce *et al.* 1984). In the context of the southern Adelaide Fold-Thrust Belt, it is the oldest of a series of granites with compositions showing progressive transition to the volcanic-arc granites field during the ensuing compressive phase of the Delamerian Orogeny. This temporal trend is followed by migration back to the within-plate granites field by the post-tectonic granites.

Although the syntectonic granites fall into the volcanic-arc granites field (Pearce *et al.* 1984), there is no other compelling evidence for subduction-related activity in or near the Adelaide Fold-Thrust Belt (although contemporaneous arc activity is recorded ~300 km east in western Victoria). As we have articulated based on the evidence that Nd and Sr isotopic compositions vary with geochemical concentration (Figure 7), the granitic rocks of the Adelaide Fold-Thrust Belt reflect the product of crust–mantle interaction (assimilation–fractional crystallisation processes: DePaolo *et al.* 1992). Since their composition reflects variable crustal contamination of contemporary mafic magmas they may be expected to bear similarities to granites

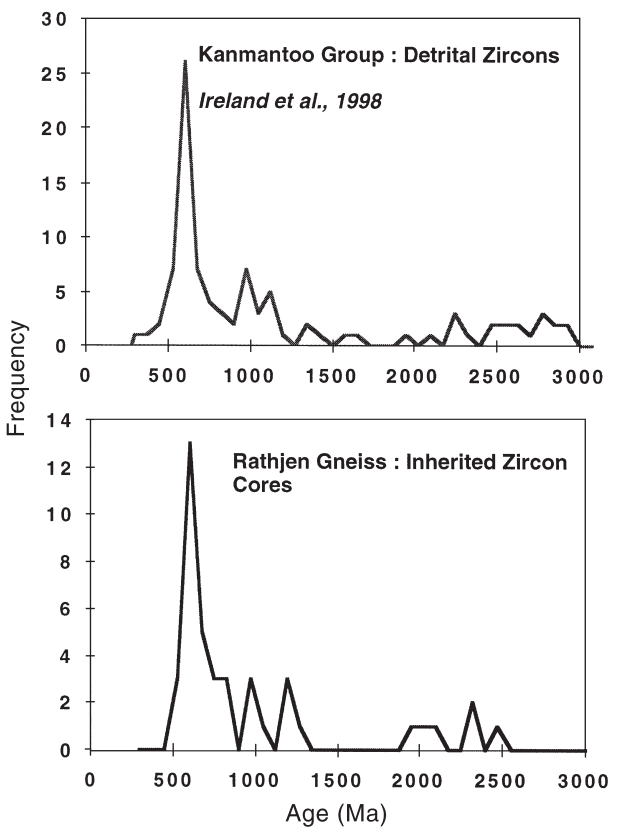

Figure 11 Plot of the age frequency of detrital zircon ages from the Kanmantoo Group (Ireland *et al.* 1998) compared with the combined (Kober and SHRIMP) inherited zircon age population from the Rathjen Gneiss.

from active arc settings, where mantle-derived magmas clearly interact with continental crust. In fact we may conclude that the granitic discrimination diagrams devised by Pearce *et al.* (1984) may be incapable of discerning granites which are assimilation–fractional crystallisation-driven continental crust-contaminated mantle magmas from those of truly subduction-related volcanic-arc origin. On the other hand, as illustrated by this study from the southern Adelaide Fold-Thrust Belt, these discriminations distinguish very accurately between granites of orogenic origin and the anorogenic (Figure 5) post-tectonic granites, which are much closer to the mantle isotope field and are mainly fractionation products of mantle melts (Figures 6, 7).

The crustal end-member may be identified using Nd and Sr isotope data (Figure 6) and the ages of inherited zircons. Their Nd–Sr isotope composition indicates that even the most S-type crust-dominated granites have Nd or Sr isotope compositions that are respectively no lower or higher than the Kanmantoo Group sedimentary rocks, having significantly lower Sr and higher Nd isotopic ratios than the Gawler Craton basement (Figure 6). In common with other syntectonic granites from the belt, the Rathjen Gneiss has inherited zircons whose ages are in the range 1200–550 Ma (Figure 11) and which are the same as detrital zircons in the Kanmantoo Group clastic sedimentary rocks. They are unlike zircons from the Gawler Craton or other adjacent exposed Proterozoic cratonic regions, where zircons have age frequency maxima between 2400 Ma and 1590 Ma. (Foden 1996).

DISCUSSION

The combination of new geochronological, structural and geochemical data for the Rathjen Gneiss provide important new constraints on the tectonic development of the southern Adelaide Fold-Thrust Belt, and imply a more complex evolution than hitherto understood.

The new dates are consistent with previous age constraints, which place the deposition of the Normanville Group at 526 ± 4 Ma (Cooper *et al.* 1992), and with an estimate of 510 ± 2 Ma for the age of the D_2 deformation (Chen & Lui 1996). The relationship between the intrusion of the Rathjen Gneiss and initiation of deformation (D_1) in the orogen remains problematic. Field relationships allow the Rathjen Gneiss to pre-date the development of the subhorizontal foliation and associated north–south-trending stretching lineation, although most recent workers have regarded it more likely that the Rathjen Gneiss is a truly syntectonic granite (Sandiford *et al.* 1992, 1995; Oliver & Zakowski 1995). The arguments for this remain essentially circumstantial. For example, Sandiford *et al.* (1992, 1995) have argued that the elevated P–T conditions associated with the D_1 deformation fabrics (600–650°C at ~400 MPa) require input of heat by magmas (see also Sandiford *et al.* 1991). Furthermore, Sandiford *et al.* (1992) argued that the initiation of crustal thickening in the orogen was coincident with and responsible for the transition in the composition of contemporary high-level crustal magmatism from mafic to felsic. In this scenario the emplacement of the Rathjen Gneiss effectively marks the beginning of Delamerian orogenic activity. This interpretation and the new data imply that deposition, burial and heating of the Kanmantoo Group occurred in a relatively short interval (between 526 ± 4 and 514 ± 4 Ma). Together with constraints on age of emplacement of the post-tectonic granites at 490–480 Ma (Turner *et al.* 1996), it also provides a maximum duration for the Delamerian orogeny of ~35 million years.

The S_1 subhorizontal foliation and associated L_1 north–south-trending stretching lineations found in the Rathjen Gneiss and in the enclosing migmatitic metasediments, provide interesting insight into the tectonic complexity of the belt. As discussed earlier, this fabric is kinematically distinct from fabrics resulting from subsequent upright folding during east–west shortening and which are probably associated with the development of westward-verging thrust-stacking in the more external lower grade parts of the belt (Jenkins & Sandiford 1992; Flöttmann *et al.* 1994, 1995). The possibility that these fabrics are due to an early phase of north–south extensional deformation has been argued by Oliver and Zakowski (1995). We also note that the association of relatively deep-water sedimentation and mafic magmatism of the type observed in the Kanmantoo basin prior to *ca* 520 Ma probably indicates lithospheric extension and rifting.

Emerging from this study is an interpretation of a more complex structural evolution than the traditional view of east–west convergence and shortening (Flöttmann *et al.* 1994, 1995). Both structural and magmatic histories imply the juxtaposition of extensional and compressional tectonic regimes over relatively short time intervals. Zircon geochronology and Nd–Sr isotope studies each imply that the deep crustal component of these granite sources does not include Palaeoproterozoic to Mesoproterozoic rocks. This suggests that the Kanmantoo basin conceals an important lithospheric structure characterised by younger mean crustal ages to the east. As simple closure of a pre-Delamerian rift from direct reversal and convergence on the original extensional vectors would be expected to return South Australian autochthonous basement from the east, the change in detrital zircon ages of Kanmantoo basin fill must support the translation of a new younger crustal source terrain from the southeast. A combination of some element of oblique convergence on this boundary, coupled with variable geometry from north to south, may lead to periodic local transition from extension to compression perhaps indicative of a transpressional regime as suggested by Flöttmann *et al.* (1995). Indeed, such a scenario would provide an ideal environment to produce variations in the interaction of mantle-derived magmas with, and fractionation in, the crust required to yield the variety of granite chemistries observed in the southern Adelaide Fold-Thrust Belt.

ACKNOWLEDGEMENTS

We thank W. Preiss, T. Flöttmann, S. Turner, S. F. Lui and Andy Burtt for their constructive and helpful discussion over the years. We acknowledge informed and constructive reviews by Alec Trendall and Nick Oliver. We also thank J. Stanley, S. Proferes and D. Bruce in the Department of Geology and Geophysics, University of Adelaide for their

assistance, and S. Stowe of the Australian National University Electron Microscopy Unit and N. Gabbitas for assistance with cathodoluminescence imaging.

REFERENCES

Chen Y. D. & Lui S. F. 1996. Precise U–Pb zircon dating of a post-D2 meta-dolerite: constraints for rapid tectonic development of the southern Adelaide Fold Belt during the Cambrian. *Journal of the Geological Society of London* **153**, 83–90.

Cooper J., Jenkins R. J. F., Compston W. & Williams I. S. 1992. Ion probe dating of a tuff in the South Australian Lower Cambrian. *Journal of the Geological Society of London* **149**, 185–192.

Chapman H. J. & Roddick J. C. 1994. Kinetics of Pb release during the zircon evaporation technique. *Earth and Planetary Science Letters* **121**, 601–611.

Cocherie A., Guerrot C. & Rossi Ph. 1992. Single-zircon dating by stepwise Pb evaporation: comparison with other geochronological techniques applied to the Hercynian granites of Corsica, France. *Chemical Geology (Isotope Geoscience Section)* **101**, 131–141.

Coney P. J., Edwards A., Hine R., Morrison F. & Windrim D. 1990. The regional tectonics of the Tasman orogenic system, eastern Australia. *Journal of Structural Geology* **12**, 519–543.

Daily B. & Milnes A. R. 1973. Stratigraphy, structure and metamorphism of the Kanmantoo Group (Cambrian) in its type section east of Tunkallilla Beach, South Australia. *Transactions of the Royal Society of South Australia* **97**, 213–242.

DePaolo D. J., Perry F. V. & Baldridge W. S. 1992. Crustal versus mantle sources of granite magmas: a two-parameter model based on Nd isotopic studies. *Transactions of the Royal Society of Edinburgh* **83**, 439–446.

Dougherty-Page J. S. & Foden J. 1996. A Pb–Pb zircon evaporation date for the Charleston Granite: comparisons with other zircon geochronology techniques. *Australian Journal of Earth Sciences* **43**, 133–138.

Fanning C. M. 1990. Single grain dating of a granite sample from Cape Willoughby, Kangaroo Island. Prise Laboratories, Australian National University Progress Report 89-060. *Department of Mines and Energy South Australia Open File Envelope* **8828**, 29–32.

Fleming P. D. & White A. J. R. 1984. Relationships between deformation and melting in the Palmer migmatites. *Australian Journal of Earth Sciences* **31**, 351–360.

Flöttmann T., James P., Rogers J. & Johnson T. 1994. Early Palaeozoic foreland thrusting and basin reactivation at the Palaeo-Pacific margin of the southeastern Australian Precambrian Craton: a reappraisal of the structural evolution of the southern Adelaide Fold-thrust Belt. *Tectonophysics* **234**, 95–116.

Flöttmann T., James P., Menpes R. *et al*. 1995. Kangaroo Island, South Australia: strain and kinematic partitioning during Delamerian basin and platform reactivation. *Australian Journal of Earth Sciences* **42**, 35–49.

Foden J. D., Turner S. P. & Morrison R. 1990. The tectonic implications of the Delamerian magmatism in South Australia and western Victoria. *In:* Jago J. B. & Moore P. S. eds. *The evolution of a Late Precambrian–Early Palaeozoic Rift Complex: The Adelaide Geosyncline,* pp. 483–495. Geological Society of Australia Special Publication **16**.

Foden J. 1996. Provenance of Neoproterozoic and early Palaeozoic sediments eastern Australia: implications from Nd isotope and zircon studies. *Geological Society of Australia Abstracts* **41**, 146.

Ireland T., Flöttmann T., Fanning M., Gibson G. & Preiss W. V. 1998. Development of the Early Palaeozoic Pacific margin of Gondwana from detrital-zircon ages across the Delamerian Orogen. *Geology* **26**, 243–246.

Jenkins R. J. F. 1990. The Adelaide Fold Belt: tectonic reappraisal. *In:* Jago J. B. & Moore P. S. eds. *The evolution of a Late Precambrian–Early Palaeozoic Rift Complex: The Adelaide Geosyncline*, pp. 396–420. Geological Society of Australia Special Publication **16**.

Jenkins R. F. J. & Sandiford M. 1992. Observations on the tectonic evolution of the southern Adelaide Fold Belt *Tectonophysics* **214**, 27–36.

Kober B. 1987. Single zircon evaporation combined with Pb^+ emitter bedding for $^{207}Pb/^{206}Pb$ age investigations using thermal ion mass spectrometry, implications to zirconology. *Contributions to Mineralogy and Petrology* **96**, 63–71.

Koschek G. 1993. Origin and significance of the SEM cathodoluminescence from zircon. *Journal of Microscopy* **171**, 223–232.

Mancktelow N. S. 1990. The structure of the southern Adelaide Fold Belt, South Australia. *In:* Jago J. B. & Moore P. S. eds. *The evolution of a Late Precambrian–Early Palaeozoic Rift Complex: The Adelaide Geosyncline*, pp. 369–395. Geological Society of Australia Special Publication **16**.

Milnes A. R., Compston W. & Daily B. 1975. Pre- to syntectonic emplacement of early Palaeozoic granites in southeastern South Australia. *Journal of the Geological Society of Australia* **24**, 87–106.

Offler R. & Fleming P. D. 1968. A synthesis of folding and metamorphism in the Mount Lofty Ranges, South Australia. *Journal of the Geology Society of Australia* **15**, 245–266.

Oliver N. H. S. & Zakowski S. 1995. Timing and geometry of deformation, low-pressure metamorphism and anatexis in the eastern Mt Lofty Ranges: the possible role of extension. *Australian Journal of Earth Sciences* **42**, 401–507.

Pearce J. A., Harris N. B. W. & Tindle A. G. 1984. Trace element discrimination diagrams for the tectonic interpretation of granitic rocks. *Journal of Petrology* **25**, 956–983.

Preiss W. V. 1987. The Adelaide Geosyncline—Late Proterozoic stratigraphy, sedimentation, palaeontology and tectonics. *Geological Survey of South Australia Bulletin* **53**.

Sandiford M., Foden J., Zhou S. & Turner S. 1992. Granite genesis and the mechanics of convergent orogenic belts with application to the southern Adelaide Fold Belt. *Transactions of the Royal Society of Edinburgh (Earth Sciences)* **83**, 83–93.

Sandiford M., Fraser G., Arnold J., Foden J. & Farrow T. 1995. Some causes and consequences of high-temperature, low-pressure metamorphism in the eastern Mt Lofty Ranges, South Australia. *Australian Journal of Earth Sciences* **42**, 233–240.

Sandiford M., Martin N., Zhou S. & Fraser G. 1991. Mechanical consequences of granite emplacement during high-T,low-P metamorphism and the origin of 'anticlockwise' PT paths. *Earth and Planetary Science Letters* **107**, 164–172.

Stacey J. S. & Kramers J. D. 1975. Approximation of terrestrial lead isotope evolution by a two-stage model. *Earth and Planetary Science Letters* **26**, 207–221.

Turner S. P. 1996. Petrogenesis of the late Delamerian gabbroic complex at Black Hill, South Australia: implications for convective thinning of the lithospheric mantle. *Mineralogy and Petrology* **56**, 51–89.

Turner S. P. & Foden J. D. 1990. The nature of mafic magmatism through the evolution of the Adelaide Fold Belt and subsequent Delamerian Orogeny. *In:* Parker A. J., Rickwood P. C. & Tucker D. H. eds. *Mafic Dykes and Emplacement Mechanisms*, pp. 431–435. Balkema, Rotterdam.

Turner S. P., Foden J. D. & Morrison R. 1992. Derivation of A-type magma by fractionation of basaltic magma and an example from the Padthaway Ridge, South Australia. *Lithos* **28**, 151–179.

Turner S. & Foden J. D. 1996. Magma mingling in late-Delamerian A-type granites at Mannum, South Australia. *Mineralogy and Petrology* **56**,147–169.

Turner S., Kelley S. P., VandenBerg A. H. M., Foden J., Sandiford M. & Flöttmann T. 1996. Source of the Lachlan fold belt flysch linked to convective removal of the lithospheric mantle and rapid exhumation of the Delamerian–Ross fold belt. *Geology* **24**, 941–944.

Williams I. S. & Claesson S. 1987. Isotopic evidence for the Precambrian provenance and Caledonian metamorphism of high grade paragneisses from the Seve Nappes, Scandinavian Caledonides, II. Ion microprobe zircon U–Th–Pb. *Contributions Mineralogy and Petrology* **97**, 205–217.

Received 18 November 1997; accepted 3 December 1998